Variable-curvature-slab molecular dynamics as a method to determine surface stress

Daniele Passerone
International School for Advanced Studies (SISSA), Via Beirut 4, I-34014 Trieste, Italy
and Istituto Nazionale di Fisica della Materia (INFM), Unità Trieste SISSA, Trieste, Italy

Erio Tosatti
International School for Advanced Studies (SISSA), Via Beirut 4, I-34014 Trieste, Italy;
Istituto Nazionale di Fisica della Materia (INFM), Unità Trieste SISSA, Trieste, Italy;
and The Abdus Salam International Centre for Theoretical Physics, P.O. Box 586, I-34014 Trieste, Italy

Guido L. Chiarotti and Furio Ercolessi
International School for Advanced Studies (SISSA), Via Beirut 4, I-34014 Trieste, Italy
and Istituto Nazionale di Fisica della Materia (INFM), Unità Trieste SISSA, Trieste, Italy
(Received 11 June 1998)

A thin plate or slab, prepared so that opposite faces have different surface stresses, will bend as a result of the stress difference. We have developed a classical molecular-dynamics (MD) formulation where (similar in spirit to constant-pressure MD) the curvature of the slab enters as an additional dynamical degree of freedom. The equations of motion of the atoms have been modified according to a variable metric, and an additional equation of motion for the curvature is introduced. We demonstrate the method to Au surfaces, both clean and covered with Pb adsorbates, using many-body glue potentials. Applications to stepped surfaces, deconstruction, and other surface phenomena are under study. [S0163-1829(99)10311-4]

I. INTRODUCTION

There has recently been a reevaluation of the role of surface stress, as an important microscopic indicator of the state of a crystal surface. Recent experimental and theoretical aspects of issues related to surface stress were reviewed by Ibach.[1]

A good example of connection between microscopic and macroscopic quantities is the determination of surface stress from the measurement of macroscopic deformations of a thin plate-shaped sample. According to elasticity theory,[2] if a thin plate presents a stress difference between its two surfaces, it will bend in order to minimize its total free energy. In the limit of small deformations, a simple formula connects the stress difference, thickness, curvature, and elastic properties of the sample. Several methods have been recently used to measure the bending. They are mainly optical or based on scanning tunneling microscopy (STM).[1] Flinn, Gardner, and Nix[3] discussed a laser scanning technique to measure the stress-induced curvature, and presented experimental results for stress in Al-Si films as a function of temperature. Martinez, Augustyniak, and Golovchenko[4] measured surface-stress changes resulting from monolayer and submonolayer coverages of gallium on Si(111). They used local-density-approximation calculations of stress in the Ga-covered Si(111) for a determination of stress in the Si(111) 7×7 and Si(Ga) superlattice surfaces. Stress variations associated with deconstruction of Au(111) and Au(100) were obtained by STM.[5,6] Moreover, the influence of adsorbates on surface stress has been exploited using the sample bending method for C/Ni(111),[7] S/Ni(111),[8] Co/Ni(100),[9] K/Pt(111),[10] Co/Pt(111),[11] and Ag/Pt(111).[12]

An atomistic simulation method which controls the curvature of a sample as an extra degree of freedom has not been available so far, although this would seem a potentially useful tool. The situations in which surface stress varies when physical phenomena occur at interfaces are numerous: adsorbates, reconstructions, steps, and phase transitions can change surface stress dramatically. All of these phenomena are, under some conditions, well described by suitable molecular-dynamics (MD) simulations. A simulation method, where the slab curvature can be measured as a function of adsorbate coverage, should represent a powerful connection between important microscopic and macroscopic quantities.

In this work we describe and demonstrate a scheme which is meant to fill this gap. It is a classical MD method, but it could in principle be extended to *ab initio* MD calculations. It is based on extending the usual concept of variable cell MD, pioneered by Andersen[13] and by Parrinello and Rahman,[14] to a slab with variable curvature. In our formulation the curvature is a single, global, Lagrangian degree of freedom. Surface stress can be extracted as a direct result of the calculation through elasticity equations,[15] which will be described below.

The outline of the work is as follows: Sec. II will present the theory and geometric considerations underlying our simulation. In Sec. IV, the phenomenology of a bent plate is reviewed in order to extract the pertinent equations. In Sec. V we present some initial applications of the method. Finally, Sec. VI is devoted to a discussion and conclusions.

II. THEORY

In ordinary variable-cell MD, the coordinates of an atom can be written as

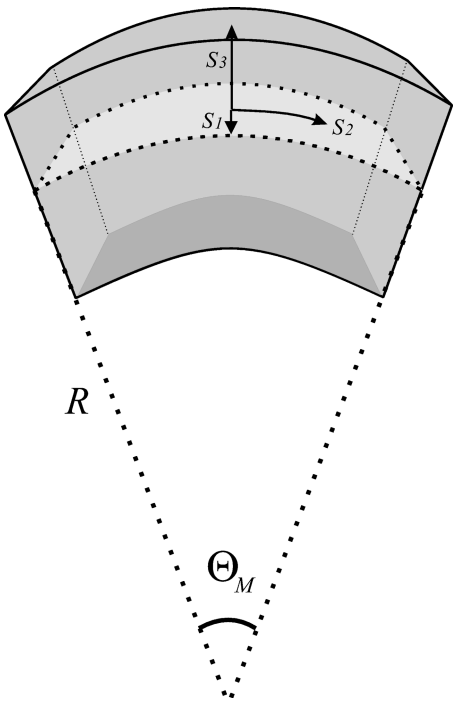

FIG. 1. The geometry of a bent plate with curvilinear coordinates; s_1 and s_2 lie in the neutral plane (shown as lighter in the figure) whereas s_3 is vertical. R is the curvature radius measured at $s_3=0$, and θ_M is the bending angle.

$$\mathbf{r}_i=\hat{\mathbf{H}}\cdot\mathbf{s}_i, \tag{1}$$

where $\mathbf{r}_i$ is the position vector of the ith particle, $\mathbf{s}_i$ are scaled coordinates ($s_i^j, j=1,\ldots,3$ are held between -0.5 and 0.5), and $\hat{\mathbf{H}}$ is a matrix describing the space metric inside the cell. Supposing, as was done by Parrinello and Rahman,[14] that the cell can vary in volume and shape, these variations can be accounted for by $\hat{\mathbf{H}}$, whose elements can be treated as an extra set of dynamical degrees of freedom. Our aim is to extend this kind of approach to the case of a bending plate, through a different choice of the metric $\hat{\mathbf{H}}$.

Let us start with a slab-shaped system, with two surfaces and lateral (x,y) periodic boundary conditions (PBC's). Suppose we bend the slab cylindrically through a radius R (see Fig. 1). A convenient choice of the transformation matrix, convenient to our problem, could be

$$\mathbf{r}=\hat{H}(\mathbf{s},R)\cdot\mathbf{s}, \tag{2}$$

where $\hat{\mathbf{H}}$, depending parametrically on the radius of curvature R, is no longer uniform (as in the Parrinello-Rahman scheme), but rather depends on the point $\mathbf{s}$. This dependence is what originates the curvature. In Fig. 1, for example, s_1 goes from -0.5 to 0.5 along x, which we choose to be unaffected by curvature; s_2 goes from -0.5 to 0.5 along direction y, which follows the curvature; and s_3 spans the sample from its inner to its outer surface.

From now on, we will use as reference surface an ideal ''neutral cylinder'' inside the slab, defined by $s_3=0$. In particular, we define the curvature k as the inverse radius of the neutral cylinder:

$$k=\left.\frac{1}{R}\right|_{s_3=0}. \tag{3}$$

In this way, if L_y is the linear dimension (arc) along the bending direction at $k=0$, the total bending angle is given by $\theta_M=L_y k$. Whereas in the Parrinello-Rahman approach the whole matrix $\hat{\mathbf{H}}$ is treated as a set of additional degrees of freedom, in our case $\hat{\mathbf{H}}$ is completely determined by the single parameter k which we will include in the Lagrangian as an extra degree of freedom.

A. Lagrangian

The next step is the construction of a Lagrangian. The general, classical Lagrangian for a N-particle interacting system is

$$L=T-V=\tfrac{1}{2}\sum_i m_i\|\dot{\mathbf{r}}_i\|^2-V(\mathbf{r}_1\ldots\mathbf{r}_N). \tag{4}$$

In Cartesian coordinates $\dot{\mathbf{r}}_i=\hat{\mathbf{H}}\cdot\dot{\mathbf{s}}_i$ and $\|\dot{\mathbf{r}}\|^2=\dot{\mathbf{s}}_i^{\mathbf{T}}\hat{\mathbf{G}}\,\dot{\mathbf{s}}_i$, where $\hat{\mathbf{G}}=\hat{\mathbf{H}}^{\mathbf{T}}\hat{\mathbf{H}}$ is the metric tensor.[14] We now define an extended Lagrangian $\tilde{L}$ by including an artificial ''curvature kinetic energy''

$$\tilde{L}=L+\tfrac{1}{2}W\dot{k}^2, \tag{5}$$

where W acts effectively as a ''curvature inertial mass.'' The velocity of a particle can be written as

$$\dot{\mathbf{r}}=\frac{d}{dt}(\hat{\mathbf{H}}\cdot\mathbf{s}), \tag{6}$$

or, explicitly,

$$\dot{r}^\alpha=\frac{d}{dt}(H_{\alpha\beta}s^\beta)=\dot{H}_{\alpha\beta}(\mathbf{s},k)\,s^\beta+H_{\alpha\beta}\dot{s}^\beta$$
$$=\left[\frac{\partial H_{\alpha\beta}}{\partial s^\gamma}\dot{s}^\gamma+\frac{\partial H_{\alpha\beta}}{\partial k}\dot{k}\right]s^\beta+H_{\alpha\beta}\dot{s}^\beta. \tag{7}$$

The third term is the usual time derivative for the constant-cell motion, whereas the second term contains a time derivative of the extra degree of freedom k. As in the Parrinello-Rahman formulation,[14] we will omit this term from the definition of the particle velocities. The kinetic energy of the system will therefore depend on $\dot{k}$ only through the curvature kinetic energy

$$\tilde{T}=\tfrac{1}{2}W\dot{k}^2, \tag{8}$$

whose interpretation is discussed in Appendix A. Parrinello and Rahman[14] and Andersen,[13] using a similar approach, showed that the equations of motion derived from their Lagrangian satisfy important requisites, leading in particular to correct thermodynamic averages (not dependent on the choice of W), and to a correct balance between external and internal stress.

One can then cast Eq. (7) as

$$\dot{r}^{\alpha}=\frac{\partial H_{\alpha\beta}}{\partial s^{\gamma}}\dot{s}^{\gamma}s^{\beta}+H_{\alpha\beta}\dot{s}^{\beta}=\left[\frac{\partial H_{\alpha\sigma}}{\partial s^{\beta}}s^{\sigma}+H_{\alpha\beta}\right]\dot{s}^{\beta}\doteq M_{\alpha\beta}\dot{s}^{\beta}. \tag{9}$$

The kinetic energy of a particle then becomes

$$T_1=\tfrac{1}{2}m\|\dot{\mathbf{r}}\|^2=\tfrac{1}{2}m\,\dot{s}^{\alpha}N_{\alpha\beta}\dot{s}^{\beta}=\tfrac{1}{2}m\,\dot{\mathbf{s}}^{\mathbf{T}}\hat{\mathbf{N}}\dot{\mathbf{s}}, \tag{10}$$

where $\hat{\mathbf{N}}\doteq\hat{\mathbf{M}}^{\mathbf{T}}\cdot\hat{\mathbf{M}}$.

We need now to express the potential energy in terms of the scaled coordinates and of the metric. In the following, we will use mostly potentials (such as pairwise potentials or many-body potentials of the ''glue'' form) which only depend on pair distances:

$$V=V(\{\|\mathbf{r}_i-\mathbf{r}_j\|^2|\,i\neq j\,;i,j=1,\ldots,N\}). \tag{11}$$

It is therefore necessary to express $\|\mathbf{r}_i-\mathbf{r}_j\|^2$ in the new coordinates.[16] Denoting the metric tensor as $\hat{\mathbf{G}}(k,\mathbf{s}_i)=\hat{\mathbf{H}}^{\mathbf{T}}(k,\mathbf{s}_i)\cdot\hat{\mathbf{H}}(k,\mathbf{s}_i)$ we have

$$\|\mathbf{r}_i-\mathbf{r}_j\|^2\equiv r_{ij}^2=\mathbf{s}_i^{\mathbf{T}}\hat{\mathbf{G}}(k,\mathbf{s}_i)\mathbf{s}_i+\mathbf{s}_j^{\mathbf{T}}\hat{\mathbf{G}}(k,\mathbf{s}_j)\mathbf{s}_j - 2\,\mathbf{s}_i^{\mathbf{T}}\hat{\mathbf{H}}^{\mathbf{T}}(k,\mathbf{s}_i)\cdot\hat{\mathbf{H}}(k,\mathbf{s}_j)\mathbf{s}_j. \tag{12}$$

We now have all the ingredients needed to write the $3N+1$ Lagrange equations

$$W\ddot{k}+\frac{\partial V}{\partial k}-\frac{1}{2}\sum_i m_i\dot{\mathbf{s}}_i^{\mathbf{T}}\frac{\partial\hat{\mathbf{N}}}{\partial k}\dot{\mathbf{s}}_i=0,$$

$$m_l\hat{\mathbf{N}}(k,\mathbf{s}_l)\ddot{\mathbf{s}}_l+\frac{\partial V}{\partial\mathbf{s}_l}-\frac{1}{2}m_l\dot{\mathbf{s}}_l^{\mathbf{T}}\frac{\partial\hat{\mathbf{N}}}{\partial\mathbf{s}_l}\dot{\mathbf{s}}_l+m_l\dot{\hat{\mathbf{N}}}(k,\mathbf{s}_l)\dot{\mathbf{s}}_l=0, \tag{13}$$

$$l=1,\ldots,N.$$

B. Construction of the $\hat{\mathbf{H}}$ matrix

To obtain an explicit form for Eqs. (2) and (13), we write the expression for the Cartesian coordinates in a box with linear dimensions (at $k=0$) L_x, L_y, and L_z:

$$x=s_1L_x,$$

$$y=\left(\frac{1}{k}+s_3L_z\right)\sin\theta,$$

$$z=s_3L_z\cos\theta+\frac{1}{k}(\cos\theta-1), \tag{14}$$

where θ is the angle running along the y direction, and $-\theta_M/2<\theta<\theta_M/2$ (see Fig. 1). With the help of simple trigonometric formulas, we can express θ in terms of s_2 and k:

$$\sin\frac{\theta}{2}=2\,s_2\sin\frac{k\,L_y}{4}, \tag{15}$$

from which Eqs. (14) become

$$x=s_1L_x,$$

$$y=4\,s_2\left(\frac{1}{k}+s_3L_z\right)\sin(k\,L_y/4)\sqrt{1-4(s_2)^2\sin^2(k\,L_y/4)},$$

$$z=s_3L_z[1-8\,(s_2)^2\sin^2(k\,L_y/4)]-\frac{1}{k}[8\,(s_2)^2\sin^2(k\,L_y/4)]. \tag{16}$$

By inspection, we see that a possible choice for $\hat{\mathbf{H}}$ is ($u=L_y/4$)

$$\hat{\mathbf{H}}(s_2,k)=\begin{pmatrix} L_x & 0 & 0\\ 0 & 4\dfrac{\sin(k\,u)}{k}\sqrt{1-4(s_2)^2\sin^2(k\,u)} & 4\,s_2L_z\sin(k\,u)\sqrt{1-4(s_2)^2\sin^2(k\,u)}\\ 0 & -s_2\dfrac{\sin^2(k\,u)}{k} & L_z[1-8\,(s_2)^2\sin^2(k\,u)]\end{pmatrix}. \tag{17}$$

It can be easily shown that Eq. (2) is verified and that, in the limit of zero curvature, $\lim_{k\to0}\hat{\mathbf{H}}(s_2,k)=\mathrm{diag}[L_x,L_y,L_z]$; that is, the Cartesian $\hat{\mathbf{H}}$ matrix is recovered. Moreover, the same equations are exact in the limit of finite, fixed curvature.

The explicit form of $\hat{\mathbf{N}}$ can be obtained by using Eqs. (10) and (17):

$$N_{\alpha\beta}=\begin{pmatrix} L_x^2 & 0 & 0\\ 0 & \dfrac{16(k\,L_z\,s_3+1)^2\sin^2(k\,u)}{[1-4(s_2)^2\sin^2(k\,u)]k^2} & 0\\ 0 & 0 & L_z^2\end{pmatrix}. \tag{18}$$

$\hat{\mathbf{N}}$ is diagonal as a consequence of the chosen cylindrical geometry.

III. CONSTRAINED MOLECULAR DYNAMICS AND PBC

The Lagrange equations are integrated using numerical methods. In particular, we will use a second-order velocity Verlet algorithm, which is at the same time well tested and simple. We found some problems due to the instability of the center of mass of the sample during the bending, which were overcome and will be commented just below.

Our starting geometry is an *n*-layer crystalline slab with PBC's along the *x* and *y* directions. The periodicity is accounted for by the scaled coordinates s_1 and s_2. The choice of coordinates we have adopted requires a slightly different set of PBC's with respect to the usual slab simulations. Along the *x* direction, nothing changes: the minimum images of a particle with scaled *x* coordinate equal to s_1 have simply the coordinates $(s_1 \pm 1)$. Along *y* (the bending direction) the requirement is that the angle θ of the particle should transform into $(\theta \pm \theta_M)$. The scaled *y* coordinate of the minimum image is then

$$s_2^{(F)} = \left(2\cos^2\frac{\theta_M}{4} - 1 \right) s_2 \pm \cos\frac{\theta_M}{4}\sqrt{1-4\,(s_2)^2\sin^2\frac{\theta_M}{4}}. \tag{19}$$

When a particle is folded into its image, we also require that its velocity should remain unchanged in modulus, its direction following the curvature of the sample. Since the components $\dot{s}_1$ and $\dot{s}_3$ do not change, the conservation of the velocity modulus is sufficient to determine $\dot{s}_2^{(F)}$:

$$\dot{\mathbf{s}}^{(F)}\,\hat{\mathbf{N}}(\mathbf{s}, k^{(F)})\,\dot{\mathbf{s}}^{(F)} = \dot{\mathbf{s}}\,\hat{\mathbf{N}}(\mathbf{s},k)\,\dot{\mathbf{s}}, \tag{20}$$

which leads to

$$\dot{s}_2^{(F)} = \dot{s}_2\frac{N_{22}(\mathbf{s})}{N_{22}(\mathbf{s}^{(F)})} = \dot{s}_2\frac{\sqrt{1-4\,(s_2^{(F)})^2\sin^2\frac{\theta_M}{4}}}{\sqrt{1-4\,(s_2)^2\sin^2\frac{\theta_M}{4}}}. \tag{21}$$

From the computational point of view, the quantities involved in these equations are already available, since they are also needed for the force calculation. Therefore, the impact of the PBC calculation on the total simulation time is negligible.

For $k \neq 0$ the dynamics generated by Eq. (13) does not conserve the total linear momentum along the radial direction s_3, so that a vertical drift arises as a consequence of bending. To prevent such drift, we resort to a constrained MD scheme. Constrained MD is a well-known technique, and we adopted the method used by Ryckært, Ciccotti, and Berendsen[17] and Andersen[18] for simulations of rigid molecules. The main point to be kept in mind is that constraints must be verified *exactly* at every time step, otherwise instabilities will occur. Technical details on the practical implementation of this constraint are given in Appendix B.

The general MD protocol we apply consists of either constant energy runs or constant temperature runs (up to 300 K) obtained by velocity rescaling, followed by quenching to $T = 0$. Occasionally, we also introduced a damping term in the curvature dynamics.

IV. PHENOMENOLOGY OF A BENT PLATE

Before moving on to the actual implementation, it is useful to recall some known results concerning the phenomenology, largely contained in the review by Ibach.[1] The definition of surface stress, according to Gibbs,[19] as the ''reversible work per unit area required to stretch a surface elastically,'' points out the difference of this physical quantity with respect to the surface free energy, defined as the ''reversible work per unit area to create a surface.'' Stretching a *solid* surface implies modifying the substrate, whereas a simple increase of area does not: whence the difference.

Let us start with the bulk stress tensor, whose element τ_{ij} is defined as the *i*th component of the force per unit area acting on the side (with the normal to the surface parallel to the *j*th direction) of a small cube in the sample. The corresponding surface stress tensor can be defined as the deviation of this quantity with respect to the bulk value, integrated along the surface normal:

$$\tau_{ij}^{(s)} = \int_{-\infty}^{+\infty} dz[\,\tau_{ij}(z) - \tau_{ij}^{(b)}]. \tag{22}$$

The integral gives a nonzero contribution only where the value of the stress deviates from the bulk value, i.e., at the surface.

Let us consider a rectangular-shaped sheet of thickness *t*, delimited by two identical (100) surfaces. For our purposes the following simplified construction can be put to use without loss of generality.[3] Schematize the plate at zero curvature as a ''substrate'' of thickness *t* and length *L* along x_1, plus two films adsorbed on it: film *A* on the lower part of the plate, and film *B* on the upper part. Let L_A the unconstrained length (along x_1) of film *A*, and L_B the length of film *B*. Let $L_B > L$ and $L_A < L$. In order to match the length *L* of the substrate, the film must be stretched (compressed) by an amount $\Delta L_I = L - L_I$, with $I = A,B$. The deformed film attached to an undeformed substrate does not represent a condition of minimum free energy; the free energy of the entire system can be lowered by deforming the substrate slightly so as to reduce the deformation of the film. This deformation has two components: an overall compression of the substrate, and a bending of the substrate.

It can be shown[3] that the neutral plane (i.e., the plane along which the strain is zero) can be set approximately in the middle of the sheet, and the deviations from this approximation are negligible for most cases. In the following, we will extract the conditions for the minimum free energy of the sheet, allowed to bend along a single direction. For simplicity, we will choose this to be the [100] direction (of course similar formulas can be derived for any other choice). If we denote the coordinates along the nonbending direction, the bending direction and the normal to the surface with s_1, s_2, and s_3, respectively, the situation is similar to the one depicted in Fig. 1. Each element of the sample is subject to a strain $\varepsilon_{22}(x_3)$. The change in free energy per unit area associated to this strain, of an element at height s_3 is

$$u(s_3) = \int_0^{\varepsilon_{22}(s_3)} \tau_{22}(s_3)\,d\varepsilon_{22}. \tag{23}$$

The total free energy change of the bent sample (per unit area) is

$$U=\int_{-t/2}^{+t/2} ds_3 \int_0^{\varepsilon_{22}(s_3)} \tau_{22}(s_3)\, d\varepsilon_{22}. \tag{24}$$

We can separate this integral into two surface parts and a bulk part:

$$U=U^{(s+)}+U^{(s-)}+U^{(b)}, \tag{25a}$$

$$U^{(s+)}=\int_{+(t/2)-\alpha}^{+t/2} ds_3 \int_0^{\varepsilon_{22}(s_3)} [\tau_{22}(s_3)-\tau_{22}^{(b)}]\, d\varepsilon_{22}, \tag{25b}$$

$$U^{(s-)}=\int_{-t/2}^{-(t/2)+\beta} ds_3 \int_0^{\varepsilon_{22}(s_3)} [\tau_{22}(s_3)-\tau_{22}^{(b)}]\, d\varepsilon_{22}, \tag{25c}$$

$$U^{(b)}=\int_{-t/2}^{+t/2} ds_3 \int_0^{\varepsilon_{22}(s_3)} \tau_{22}^{(b)}(s_3)\, d\varepsilon_{22}. \tag{25d}$$

The first two terms lead to the definition of surface stress in the Gibbs sense, and can be written with a good approximation:

$$U^{(s+)}+U^{(s-)}=[\tau_{22}^{(s)}(+)-\tau_{22}^{(s)}(-)]\left(\frac{k\,t}{2}\right), \tag{26}$$

where $\pm k\,t/2$ are the strains at the upper and lower surfaces.

The bulk term can be expressed using the elastic constants of the crystal. Hooke's law relates strain and bulk stress tensor components in the following ways:

$$\begin{aligned}\varepsilon_{11}&=\sigma_{11}\,\tau_{11}+\sigma_{12}\,\tau_{22},\\ \varepsilon_{22}&=\sigma_{12}\,\tau_{11}+\sigma_{11}\,\tau_{22}.\end{aligned} \tag{27}$$

In our case, $\varepsilon_{11}=0$, therefore, after introducing Young's modulus Y and Poisson's ratio ν,

$$\begin{aligned}Y&=\frac{1}{\sigma_{11}},\\ \nu&=-\frac{\sigma_{12}}{\sigma_{11}},\end{aligned} \tag{28}$$

one obtains[1]

$$\varepsilon_{22}=\frac{1-\nu^2}{Y}\,\tau_{22}. \tag{29}$$

If we substitute Eq. (29) into Eq. (25d) we obtain, after integration,

$$U^{(b)}=\frac{1}{24}\,\frac{Y}{1-\nu^2}\,k^2\,t^3, \tag{30}$$

the total free energy of the bent plate is then:

$$F=[\tau_{22}^{(s)}(+)-\tau_{22}^{(s)}(-)]\left(\frac{k\,t}{2}\right)+\frac{1}{24}\,\frac{Y}{1-\nu^2}\,k^2\,t^3. \tag{31}$$

Minimizing F with respect to the curvature, one obtains the equation relating the equilibrium curvature k_M to the difference in surface stress between upper and lower surfaces:

$$\Delta\tau^{(s)}=-\frac{Y}{6\,(1-\nu^2)}\,k_M\,t^2, \tag{32}$$

where Y is the Young's modulus, ν the Poisson's number, k_M the curvature, and t the thickness of the sample. This relation is known as Stoney's equation, and was first derived in 1909 (except for the biaxial nature of the stress[15,1]). We stress that this formula is valid for a uniaxial bending, whereas for an isotropic bending in two directions the factor $(1-\nu^2)$ should be replaced by $(1-\nu)$. Another limit of validity is that the plate must be infinitely large, relative to its thickness. In other words, there will be finite thickness corrections in (t/L) where L is the lateral (x,y) size. We did not make any attempt to find these corrections so far.

In the remainder of this section we present the simple derivation of the elastic constants two high symmetry surfaces: (100) bent along [011], and (111). We start from the elastic stiffnesses C_{ij}, which are related to the compliances σ_{ij} by the equations:[20]

$$\begin{aligned}\sigma_{11}&=\frac{C_{11}+C_{12}}{(C_{11}-C_{12})(C_{11}+2\,C_{12})},\\ \sigma_{12}&=-\frac{C_{12}}{(C_{11}-C_{12})\,(C_{11}+2\,C_{12})},\\ \sigma_{44}&=\frac{1}{C_{44}}.\end{aligned} \tag{33}$$

If the uniaxial bending is not along a [100] direction and for a surface orientation other than (100), the compliances σ_{11} and σ_{12} which appear in Eq. (28) have to be replaced by effective elastic constants, which in the (100) case, with bending along a [011] direction, have the forms[21]

$$\begin{aligned}\sigma'_{11}&=\sigma_{11}-\tfrac{1}{2}(\sigma_{11}+\sigma_{12}+\tfrac{1}{2}\sigma_{44}),\\ \sigma'_{12}&=\sigma_{12}+\tfrac{1}{2}(\sigma_{11}+\sigma_{12}+\tfrac{1}{2}\sigma_{44}),\end{aligned} \tag{34}$$

whereas in the (111) case have the forms

$$\begin{aligned}\sigma'_{11}&=\sigma_{11}-\tfrac{1}{2}(\sigma_{11}+\sigma_{12}+\tfrac{1}{2}\sigma_{44}),\\ \sigma'_{12}&=\sigma_{12}+\tfrac{1}{6}(\sigma_{11}+\sigma_{12}+\tfrac{1}{2}\sigma_{44}).\end{aligned} \tag{35}$$

V. APPLICATION TO METAL SURFACES

A. Implementation

The first goal of the variable-curvature MD simulation is to obtain an equilibrium value for the curvature in order to extract the surface stress difference, according to Eq. (32). We can then compare the outcome with the surface stress difference calculated independently using Kirkwood-Buff formula,[22] and assess the success of the method. We will also verify the validity of the approach by analyzing the behavior of the curvature as a function of the slab thickness.

We will present two different exemplifications. Far from being exhaustive, these results are only meant to show the feasibility of the method in view of later applications to surface physics.

First we simulated several Au slabs with a (100) orientation and different types of reconstruction on the two sides. This test can show the sensitivity of the method: differences of the order of 5 meV/Å^2 can be appreciated. Next we examined the effect of isotropic or anisotropic adsorbates on the surface stress, as exemplified by Pb/Au(100).

All simulations were performed using many-body potentials of the glue type.[23] They have the general forms

$$V=\tfrac{1}{2}\sum_{i,\,j}\Phi(r_{ij})+\sum_{i}U(n_i),$$
$$n_i=\sum_{j}\rho(r_{ij}), \tag{36}$$

where n_i is a generalized atomic coordination. $\Phi(r)$, $U(n)$, and $\rho(r)$ are empirically constructed, by fitting several properties of the system. Well-tested glue potentials are available[24] for Au (Ref. 23) and Pb.[25] This scheme can be extended to binary systems by introducing a mixed two-body potential $\Phi_{AB}(r)$, and assuming n_i to be a linear superposition of density contributions ρ_A and ρ_B supplied, respectively, by A- and B-type atoms to site i (Ref. 26):

$$V=\frac{1}{2}\left[\sum_{i\in A}\left(\sum_{j\in A}\Phi_{AA}(r_{ij})+\sum_{j\in B}\Phi_{AB}(r_{ij})\right)+\sum_{i\in B}\left(\sum_{j\in A}\Phi_{AB}(r_{ij})+\sum_{j\in B}\Phi_{BB}(r_{ij})\right)\right]+\sum_{i\in A}U_A(n_i)+\sum_{i\in B}U_B(n_i), \tag{37}$$

with

$$n_i=\sum_{j\in A}W_A\rho_A(r_{ij})+\sum_{j\in B}W_B\rho_B(r_{ij}), \tag{38}$$

where W_A and W_B are suitable weights. In our case $W_{\mathrm{Au}}=1.045$ and $W_{\mathrm{Pb}}=0.957$.

B. A clean surface: Change of surface stress with reconstruction

We prepared a family of Au(100) slabs composed by about 600 atoms per layer ($L_x=28.78$ Å, $L_y=172.69$ Å), and different thicknesses of 8, 12, 16, and 20 layers, with [011] as the bending direction. In order to extract numerical values for the surface stress from Eq. (32), we need the correct elastic constants for this case. For the case of Au (as described by the glue model), the elastic stiffnesses have been calculated,[23] giving

$$C_{11}=2.203\times10^7\ \mathrm{N/cm^2},$$
$$C_{12}=1.603\times10^7\ \mathrm{N/cm^2}, \tag{39}$$
$$C_{44}=0.600\times10^7\ \mathrm{N/cm^2}.$$

With these values, using Eqs. (28) and (34), the Young's modulus and the Poisson's ratio for Au(100), with bending along [011], are $Y_{(100)}=1.322\times10^7$ N/cm^2 and $\nu_{(100)}=0.1022$.

Both (100) surfaces were prepared in the reconstructed state, characterized by a close-packed triangular overlayer on a square substrate. We chose a fixed reconstructed 1×5 structure (six [011] rows on top of five) for the reference (lower) surface of the plate, and we changed the nature of the upper surface, ranging from 1×3 (i.e., four surface rows over three substrate rows, a ''compressive'' situation) to a 1×20 structure (a ''tensile'' situation), touching the 1×4, 1×5, 1×6, 1×10, 1×12, and 1×15 structures. In the 1×5 case no bending was expected or observed, since the surfaces on the two sides were identical. We also considered 11×3, 11×4, $11\times5,\ldots,$ obtained by adding $[01\bar{1}]$ rows. The lowest energy surface in the glue model is 34×5,[27] in the experiment is close to 28×5, but all $M\times5$ surfaces differ very slightly in free energy.[28–31] The essential point here will be that surfaces which differ only very little in energy, for example 1×5 (102.3 meV/Å^2) and 1×12 (103.2 meV/Å^2) may differ enormously in surface stress. A typical snapshot of the simulation is shown in Fig. 2.

Figure 3 shows the time evolution of the curvature k, for two different values of the inertial parameter W. Starting from an arbitrary value, the slab curvature reaches its equilibrium value very rapidly. We verified that, as it should be and as can be seen from the figure, the value of the mass W is irrelevant in determining the equilibrium value of k. The choice of W does not influence equilibrium properties, which in classical mechanics do not depend on the mass of constituents.

Concerning dynamics, the value of the inertial parameter W which yields the fastest convergence is in general one, which gives rise to an oscillation period for k which is closest to the main physical oscillation mode of the system, since in that case the coupling of the two systems is optimal. The frequency of any particular normal mode for a plate from theory of elasticity,[32] is

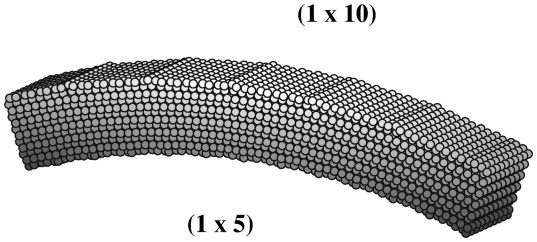

FIG. 2. A typical snapshot of the simulation, with a positive value of the curvature. The top surface is a 1×10 surface, and the lower surface a 1×5 surface, both hexagonally reconstructed Au(100). The corrugations of both surfaces are evident. This particular sample will invert its curvature during the simulation, and the equilibrium value of k will become negative.

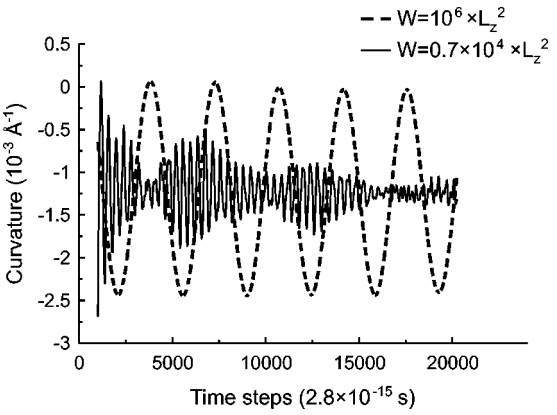

FIG. 3. Time evolution of the curvature k for two different values of the ''mass'' W. The faster case (continuous line) is close to the optimal coupling with the atomic degrees of freedom, and a beat with the normal modes of the plate appears.

$$\omega_1 = \sqrt{\frac{1}{3}\left(\frac{Y}{(1-\nu^2)\rho}\right)t^2\alpha a^4}, \tag{40}$$

where ρ is the mass density of the system, a^2 is comparable with $L_x \times L_y$, and α (dimensionless) is the solution of certain transcendental equations (it is of the order of 10 for the lowest modes). The lowest frequencies for the case shown in Fig. 3 are close to 0.1 GHz.

Figure 3 shows the comparison between a value of W leading to a low frequency for k (dashed line) and a value of W leading to a frequency close to the optimal one (continuous line). A beat with the normal modes of the plate appears in the latter case. The oscillating frequency for k is, in the weak coupling limit, proportional to $W^{1/2}$.

In the 1×3 and 1×4 cases, the equilibrium k was positive, whereas in the other cases it was negative. The simulation was performed at low temperature (from a few degrees to 300 K). The difference in surface stress between upper and lower surface has been extracted using Eq. (32). The surface stress of the two isolated surfaces has been independently obtained from MD forces using the standard Kirkwood-Buff formula.[22] The comparison of the stress differences is excellent, as can be seen from Fig. 4, showing that the variable curvature method works. The only deviation is for 1×3, and clearly attributable to excessive curvature.

The calculation is repeated with a variety of different unit cells in the top surface; by adding a $[01\bar{1}]$ row every ten, we obtain 11×3, 11×4, $11\times5, \ldots$ unit cells instead of 1×3, $1\times4,1\times5, \ldots$. The lower 1×5 surface of the slab was left unchanged. The stress variations are clearly very large, both relative to the basic stress of 1×5 (203.12 meV/Å^2) and to the surface energy ($\sim$100 meV/Å^2). We judge that the smallest surface stress difference detectable with our kind of simulation is of the order of 10 meV/Å^2. This sensitivity should be very important in the study of phase transitions.

We have also verified the linear dependence of the curvature from the inverse square of the thickness predicted by Eq. (32). Figure 5 shows the fit with 8, 12, 16, and 20 layers, and the agreement is rather good.

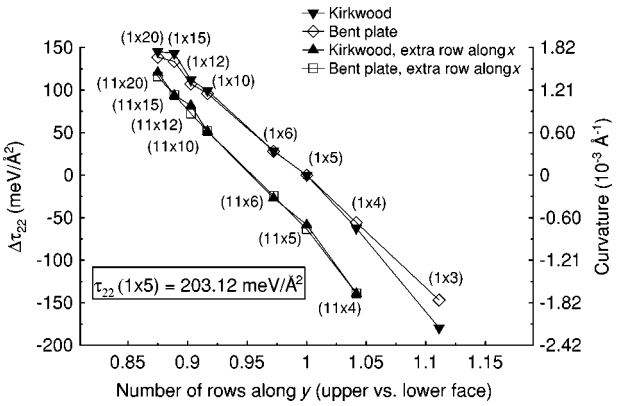

FIG. 4. Comparison between variable curvature simulations and Kirkwood-Buff formula, with different structures at the upper surface of the sample. The lower surface is a 1×5 surface in every case. Right ordinate axis: equilibrium value for the curvature. Left ordinate axis: corresponding difference in surface stress, according to Stoney's equation. In order to obtain the absolute value of the surface stress component τ_{22} of the upper surface, the reference 1×5 result (203.12 meV/Å^2) has to be added.

C. Change of surface stress with adsorption

The surface stress is obviously a strong function of adsorption. As an example, here we will consider Pb on Au. Underpotential deposition[33] has recently been used together with STM techniques to exploit the formation of two-dimensional phases of Pb on a substrate of Ag(100) and Au(100). Through different electrochemical potentials, one can obtain different phases, such as Au(100)$-c(2\times2)$ Pb, Au(100) $c(3\sqrt{2}\times\sqrt{2})R45°$ Pb, and Au(100) $c(6\times2)$ Pb. In particular, a close-packed layer of lead shows a slight contraction in both [011] directions of the quadratic substrate lattice; the final structure is pinned to the substrate lattice at equivalent adsorption sites, leading to an Au(100) $-c(6\times2)$ moiré superstructure.

Using the potential in Eq. (37), we found precisely this $c(6\times2)$ superstructure as a local-energy minimum, through quenching of a sample prepared with a perfect substrate of Au(100), and a triangular overlayer of Pb with the same density of a bulk (111) layer. In the optimized structure, the 6×2 pattern is evident [Fig. 6(a)]. Domain walls appear as

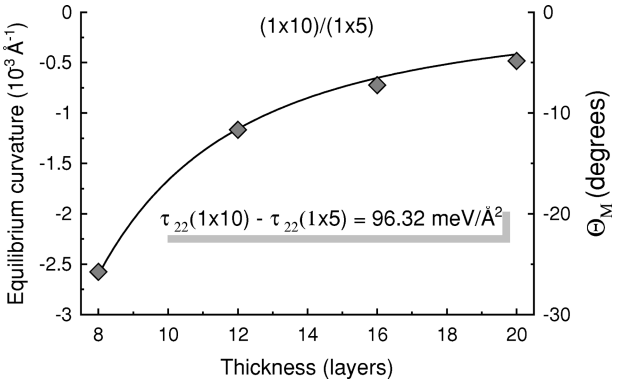

FIG. 5. Dependence of the curvature upon thickness in the case of a $(1\times10)/(1\times5)$ surface. The inverse square dependence predicted by Stoney's equation is recovered, and the stress difference is extracted from the fit.

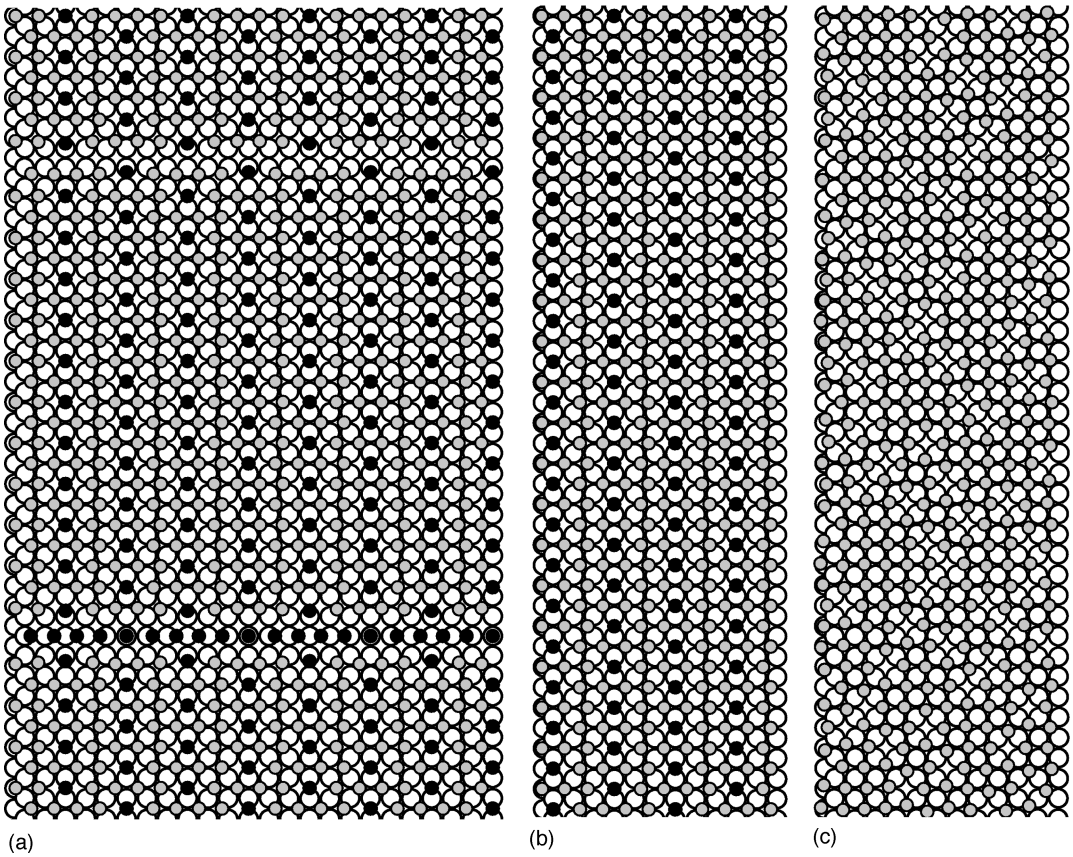

FIG. 6. Different structures for the Pb overlayer (gray and black atoms) over a square Au(100) substrate (white atoms). (a) 6×2 structure with domain walls. Black atoms are higher; two MD boxes are shown along x. (b) 6×2 structure without domain walls. (c) Square adlayer with vacancies.

the result of overlayer contraction. We were able to obtain a perfect 6×2 pattern [Fig. 6(b)] by starting from an initial configuration with a denser overlayer. Deeper energy minima are obtained by the simple commensurate square overlayers with vacancies, as in the case shown in Fig. 6(c).

We performed variable curvature simulations on both the imperfect and the perfect $c(6\times2)$ structure, and on the square overlayer with vacancies, with Au(100) (1×4) as the reference ($\tau_{22}=147.52$ meV/Å^2). For $c(6\times2)$, which is anisotropic, two different simulations were carried out in order to access separately τ_{11} and τ_{22} (the adlayer was rotated of 90°, so as to keep τ_{22} as reference).

For a 6×2 structure with domain walls, we found $\tau_{22}=88.10$ meV/Å^2 (τ_{11} was not measured in this case), and for the perfect 6×2 structure $\tau_{11}=72.41$ meV/Å^2 and $\tau_{22}=38.52$ meV/Å^2. For the square structure with vacancies, we found $\tau_{22}=40.34$ meV/Å^2. The stress anisotropy is therefore large, and the effect of the domain walls is also remarkable.

VI. CONCLUSIONS

In this work we have introduced a variable curvature slab simulation method which represents a promising technique to study properties of crystal surfaces, in particular surface stress differences. The first tests of the method, based on the comparison with known results, reveal a good accuracy, in the range of 10 meV/Å^2, and easy applicability. We are now considering studies of a variety of phenomena, including surface phase transitions, using this approach.

ACKNOWLEDGMENTS

We would like to thank Francesco Di Tolla for useful discussions and help. We acknowledge support from EU through Contracts Nos. ERBCHBGCT920180, ERBCHBGCT940636, and ERBCHRXCT930342, from INFM through PRA LOTUS, and from MURST—''Progetti di ricerca di rilevante interesse nazionale.''

APPENDIX A: INTERPRETATION OF THE KINETIC ENERGY OF THE CURVATURE

If the arc $s_3=0$ is forced to have length L_y during the whole simulation, the volume Ω of the sample is guaranteed to remain constant and equal to $L_xL_yL_z$. This is easily seen by performing the integral in polar coordinates. The difference in surface area between upper and lower layer is of course

$$\Delta A=L_x\left[\theta_{MAX}\left(R+\frac{L_z}{2}\right)-\theta_{MAX}\left(R-\frac{L_z}{2}\right)\right]$$
$$=L_xL_z\theta_{MAX}=L_xL_yL_z\,k=\Omega\,k. \tag{A1}$$

The relative time variation of this area is

$$\frac{d}{dt}\left(\frac{\Delta A}{\overline{A}}\right)=\frac{V}{L_x L_y}\frac{d}{dt}k=L_z\dot{k}. \tag{A2}$$

Therefore, the fictitious kinetic energy term is

$$\tilde{T}=\frac{1}{2}W\dot{k}^2=\frac{1}{2}\left(\frac{W}{L_z^2}\right)\left[\frac{d}{dt}\left(\frac{\Delta A}{\overline{A}}\right)\right]^2=\frac{1}{2}\left(\frac{W}{\Omega^2}\right)\left(\frac{d}{dt}(\Delta A)\right)^2. \tag{A3}$$

This result is simple but important because it allows a connection with Andersen molecular dynamics:[13] whereas in Andersen's formulation the extra degree of freedom is the volume Ω and the term $\frac{1}{2}W\dot{\Omega}^2$ is the kinetic energy tied to volume variations, in this case there is a variation in the area difference between the two faces of the sample. The analogy could be brought further, adding to our Lagrangian a term $-P\,k$, which is the reversible work of a radial force decaying as the square of the curvature radius, acting identically on all particles, whereas the term $-P\,\Omega$ in Andersen's formulation is the reversible work of the hydrostatic pressure during the variation of the cell volume. Such an external force, acting as a torque, could be used to force the equilibrium curvature to a different value from the one suggested by stress imbalance between the two surfaces. Applications of this point are presently under study.

APPENDIX B: CONSTRAINED DYNAMICS FOR FIXING THE CENTER OF MASS

1. Velocity Verlet algorithm as a predictor-corrector

Following Ref. 34, it is possible to cast a particular velocity Verlet algorithm as a predictor-corrector algorithm. One can start from

$$\begin{aligned}\mathbf{r}_0(t+\delta t)&=\mathbf{r}_0(t)+\mathbf{r}_1(t)+\mathbf{r}_2(t),\\ \mathbf{r}_1(t+\delta t)&=\mathbf{r}_1(t)+\mathbf{r}_2(t)+\mathbf{r}_2(t+\delta t),\end{aligned} \tag{B1}$$

where, as usual,

$$\mathbf{r}_n(t)=\frac{1}{n!}(\delta t)^n\frac{d^n\mathbf{r}_0}{dt^n}. \tag{B2}$$

This can be written as a two stages predictor-corrector, with a force evaluation in between:

$$\begin{aligned}\mathbf{r}_0(t+\delta t/2)&=\mathbf{r}_0(t)+\mathbf{r}_1(t)+\mathbf{r}_2(t),\\ \mathbf{r}_1(t+\delta t/2)&=\mathbf{r}_1(t)+\mathbf{r}_2(t),\\ \mathbf{r}_0(t+\delta t)&=\mathbf{r}_0(t+\delta t/2),\\ \mathbf{r}_1(t+\delta t)&=\mathbf{r}_1(t+\delta t/2)+\mathbf{r}_2(t+\delta t),\end{aligned} \tag{B3}$$

where $\mathbf{r}_2(t+\delta t)$ is obtained by the equations of motion. In this case the predicted values for the positions coincide with the corrected ones, whereas the velocities are corrected (a second-order, or three-value, predictor-corrector).

When constraints are present, the forces acting on the ith particle can be written as

$$\mathbf{F}_i=\mathbf{f}_a+\mathbf{g}_a\approx\mathbf{f}_a+\mathbf{g}_a^{(x)}. \tag{B4}$$

The constraints forces $\mathbf{g}_a$ at each stage are approximated with $\mathbf{g}_a^{(x)}$, where $(x)=r,v$, so as to ensure that the positions and the velocities, respectively, satisfy the constraints, and the quantities at the various stages have to be corrected to keep into account the constraints forces.

2. Bent plate case

In the case of varying curvature molecular dynamics, the bending leads to a drift toward the center of curvature of the center of mass. In order to fix the s_3 component of the center of mass in the origin, the only constraint to be satisfied is (assuming all the particles to have the same mass for sake of simplicity)

$$\sigma\equiv\sum_{i=1}^{N}s_{3i}=0, \tag{B5}$$

where s_{3i} are the scaled coordinates in our curvilinear system [in this appendix, s, $\dot{s}$, and $\ddot{s}$ are normalized according to Eq. (B2)]. The time derivative of the constraint equation gives a constraint on velocities:

$$\dot{\sigma}\equiv\frac{1}{\delta t}\sum_{i=1}^{N}\dot{s}_{3i}=0. \tag{B6}$$

The Lagrangian must then be completed with a term $\lambda_R\sum_{i=1}^{N}s_{3i}+\lambda_V\sum_{i=1}^{N}\dot{s}_{3i}$.

Two different approximations to the constraint forces have to be chosen so that positions and velocities satisfy the constraints exactly. In this particular case the forces turn out to be simple constants:

$$\begin{aligned}g_{3i}^{(r)}&=-\lambda_R,\\ g_{3i}^{(v)}&=-\lambda_V.\end{aligned} \tag{B7}$$

The first equation, involving positions, is

$$s_{3i}(t+\delta t)=s_{3i}(t)+\dot{s}_{3i}(t)+\ddot{s}_{3i}(t)-\frac{(\delta t)^2}{2m_i}\lambda_R. \tag{B8}$$

λ_R has to be chosen in order to satisfy the position constraint at time $t+\delta t$:

$$\begin{aligned}\sum_{i=1}^{N}\left(s_{3i}(t)+\dot{s}_{3i}(t)+\ddot{s}_{3i}(t)-\frac{(\delta t)^2}{2m_i}\lambda_R\right)&=0,\\ \lambda_R&=2m_i\frac{\sum_{i=1}^{N}\left[s_{3i}(t)+\dot{s}_{3i}(t)+\ddot{s}_{3i}(t)\right]}{N(\delta t)^2}.\end{aligned} \tag{B9}$$

Therefore the former equation becomes

$$s_{3i}(t+\delta t)=s_{3i}(t)+\dot{s}_{3i}(t)+\ddot{s}_{3i}(t)-\frac{\sum_{j=1}^{N}\left[s_{3j}(t)+\dot{s}_{3j}(t)+\ddot{s}_{3j}(t)\right]}{N}. \tag{B10}$$

The second equation, involving velocities, is

$$\dot{s}_{3i}(t+\delta t)=\dot{s}_{3i}(t)+\ddot{s}_{3i}(t)-\frac{(\delta t)^2}{2m_i}\lambda_R+\ddot{s}_{3i}(t+\delta t)-\frac{(\delta t)^2}{2m_i}\lambda_V. \tag{B11}$$

λ_V must satisfy

$$\sum_{i=1}^{N}\left(\dot{s}_{3i}(t)+\ddot{s}_{3i}(t)-\frac{\sum_{j=1}^{N}[s_{3j}(t)+\dot{s}_{3j}(t)+\ddot{s}_{3j}(t)]}{N}+\ddot{s}_{3i}(t+\delta t)-\frac{(\delta t)^2}{2m_i}\lambda_V\right)=0, \tag{B12}$$

$$\lambda_V=2m_i\frac{\sum_{i=1}^{N}[\ddot{s}_{3i}(t+\delta t)-s_{3i}(t)]}{N(\delta t)^2}$$

and the equation becomes

$$\dot{s}_{3i}(t+\delta t)=\dot{s}_{3i}(t)+\ddot{s}_{3i}(t)-\frac{\sum_{i=1}^{N}[s_{3i}(t)+\dot{s}_{3i}(t)+\ddot{s}_{3i}(t)]}{N}+\ddot{s}_{3i}(t+\delta t)-\frac{\sum_{j=1}^{N}[\ddot{s}_{3j}(t+\delta t)-s_{3j}(t)]}{N}. \tag{B13}$$

[1] H. Ibach, Surf. Sci. Rep. **29**, 193 (1997).

[2] L. Landau, *Theory of Elasticity*, 2nd ed. (Pergamon, Oxford, 1970).

[3] Paul A. Flinn, Donald S. Gardner, and William D. Nix, IEEE Trans. Electron Devices **34**, 689 (1987).

[4] R. E. Martinez, W. M. Augustyniak, and J. A. Golovchenko, Phys. Rev. Lett. **64**, 1035 (1990).

[5] C. E. Bach, M. Giesen, H. Ibach, and T. L. Einstein, Phys. Rev. Lett. **78**, 4225 (1997).

[6] H. Ibach, C. E. Bach, M. Giesen, and A. Grossmann, Surf. Sci. **375**, 107 (1997).

[7] A. Grossmann, W. Erley, and H. Ibach, Surf. Sci. **337**, 183 (1995).

[8] M. Foss, R. Feidenhansl, M. Nielsen, E. Findeisen, R. L. Johnson, T. Buslaps, I. Stensgaard, and F. Besenbacher, Phys. Rev. B **50**, 8950 (1994).

[9] A. Grossmann, W. Erley, and H. Ibach, Surf. Sci. **313**, 209 (1994).

[10] A. Grossmann, Thesis, RWTH Aachen D80, 1996.

[11] A. Grossmann, W. Erley, and H. Ibach, Surf. Rev. Lett. **2**, 543 (1995).

[12] A. Grossmann, W. Erley, J. B. Hannon, and H. Ibach, Phys. Rev. Lett. **77**, 127 (1996).

[13] H. C. Andersen, J. Chem. Phys. **72**, 2384 (1980).

[14] M. Parrinello and A. Rahman, J. Appl. Phys. **52**, 7182 (1981).

[15] G. G. Stoney, Proc. R. Soc. London, Ser. A **82**, 172 (1909).

[16] The extension to potentials with angular dependence, such as Tersoff potentials, of course requires a derivation of more cumbersome equations of motion, but is in principle possible.

[17] J. P. Ryckært, G. Ciccotti, and H. J. C. Berendsen, J. Comput. Phys. **23**, 327 (1977).

[18] H. C. Andersen, J. Comput. Phys. **52**, 24 (1983).

[19] J. W. Gibbs, *The Scientific Papers of J. Willard Gibbs* (Longmans-Green, London, 1906), Vol. 1, p. 55.

[20] C. Kittel, *Introduction to Solid State Physics*, 7th ed. (Wiley, New York, 1996).

[21] W. A. Brantley, J. Appl. Phys. **44**, 534 (1973).

[22] See, e.g., O. K. Rice, *Statistical Mechanics, Thermodynamics and Kinetics* (Freeman, San Francisco, 1967), Chap. 13.

[23] F. Ercolessi, M. Parrinello, and E. Tosatti, Philos. Mag. A **58**, 213 (1988).

[24] These potentials can be downloaded at the URL http://www.sissa.it/~furio/potentials/

[25] H. S. Lim, C. K. Ong, and F. Ercolessi, Surf. Sci. **269/270**, 1109 (1992).

[26] F. Ercolessi, O. Tomagnini, S. Iarlori, and E. Tosatti, in *Nanostructures and Manipulation of Atoms under High Fields and Temperatures: Applications*, edited by Vu Thien Binh, N. Garcia, and K. Dransfeld (Kluwer, Dordrecht, 1993), p. 185.

[27] F. Ercolessi, E. Tosatti, and M. Parrinello, Phys. Rev. Lett. **57**, 719 (1986); Surf. Sci. **177**, 314 (1986).

[28] K. Yamazaki, K. Takayanagi, Y. Tanishiro, and K. Yagi, Surf. Sci. **199**, 595 (1988).

[29] P. W. Palmberg and T. N. Rhodin, J. Chem. Phys. **49**, 134 (1968).

[30] T. Hasegawa, N. Ikarashi, K. Kobayashi, K. Takayanagi, and K. Yagi, in *Proceedings of the Second International Conference on the Structure of the Surfaces, Amsterdam 1987*, edited by J. F. Van der Veen and M. A. Van Hove (Springer, Berlin, 1988), p. 43.

[31] G. K. Binnig, H. Rohrer, Ch. Gerber, and E. Stoll, Surf. Sci. **144**, 321 (1984).

[32] H. Lamb, *The Dynamical Theory of Sound* (Dover, New York, 1925).

[33] U. Schmidt, S. Vinzelberg, and G. Staikov, Surf. Sci. **348**, 261 (1996).

[34] M. P. Allen and D. J. Tildesley, *Computer Simulation of Liquids* (Oxford University Press, Oxford, 1989).